TISSUE ENGINEERING

In situ expansion of engineered human liver tissue in a mouse model of chronic liver disease

Kelly R. Stevens,[1,2,3] Margaret A. Scull,[4] Vyas Ramanan,[1,2] Chelsea L. Fortin,[1,2,3] Ritika R. Chaturvedi,[5] Kristin A. Knouse,[2,6,7] Jing W. Xiao,[4] Canny Fung,[4] Teodelinda Mirabella,[8] Amanda X. Chen,[2,6] Margaret G. McCue,[9] Michael T. Yang,[10] Heather E. Fleming,[1,2] Kwanghun Chung,[1] Ype P. de Jong,[4,11] Christopher S. Chen,[5,8] Charles M. Rice,[4] Sangeeta N. Bhatia[1,2,12,13]*

Control of both tissue architecture and scale is a fundamental translational roadblock in tissue engineering. An experimental framework that enables investigation into how architecture and scaling may be coupled is needed. We fabricated a structurally organized engineered tissue unit that expanded in response to regenerative cues after implantation into mice with liver injury. Specifically, we found that tissues containing patterned human primary hepatocytes, endothelial cells, and stromal cells in a degradable hydrogel expanded more than 50-fold over the course of 11 weeks in mice with injured livers. There was a concomitant increase in graft function as indicated by the production of multiple human liver proteins. Histologically, we observed the emergence of characteristic liver stereotypical microstructures mediated by coordinated growth of hepatocytes in close juxtaposition with a perfused vasculature. We demonstrated the utility of this system for probing the impact of multicellular geometric architecture on tissue expansion in response to liver injury. This approach is a hybrid strategy that harnesses both biology and engineering to more efficiently deploy a limited cell mass after implantation.

INTRODUCTION

Advances in tissue engineering have enabled the generation of numerous tissue types that can recapitulate many aspects of native organs, bringing closer the promise that engineered tissues may ultimately replace whole-organ transplantation (*1*, *2*). However, constructing complex solid organs remains a major physical and biological challenge. For engineered tissues that can be fed by diffusion of nutrients from the environment (such as the cornea and skin), thick tissues with low metabolic requirements (such as cartilage), or small-scale endocrine tissues (such as β cells of the pancreas), the recapitulation of complex tissue architecture has not been a limiting factor for clinical translation (*1*, *2*). However, providing structural organization is likely important for large, metabolically active solid organs such as the heart, kidney, and liver. For example, the liver contains more than 100 billion hepatocytes, all positioned within 50 μm of the circulation (*3*). The organization of the circulation and its lining endothelium are integral aspects of the functional organ and are critical to the delivery of vital nutrients to the entire parenchyma of tissue, as well as to the cell-cell interactions that define juxtacrine and paracrine signals that drive diverse processes such as embryological development, organ function, and regeneration (*4*, *5*).

A variety of approaches have been examined to promote vascularization and architectural structural control of solid engineered tissues. For example, inclusion of randomly organized or patterned endothelial cells has improved both the engraftment rate and persistence of metabolic tissues (*6*–*8*). Decellularization of native structures (*9*, *10*) and biofabrication techniques, such as microtissue molding (*1*, *2*) and bioprinting (*3*–*5*), have provided further ways to organize cells into scalable vascularized architectures, but all of these approaches offer limited utility for large solid organs because tissues must be perfused rapidly (within ~1 hour of tissue assembly) to prevent ischemic injury.

A different approach may be to nucleate a "seed" of an organ derived from mature cell populations that can grow by in situ expansion, as seen both in hepatic embryogenesis wherein primordial tissue buds grow into vascularized organs and in regenerative adult responses wherein hepatocytes and their vasculature undergo coordinated expansion (*6*–*9*). As a step toward this goal, cells have been expanded after engraftment in solid organs by manipulating cell signaling pathways (*10*–*12*) or by creating a repopulation advantage for graft cells using injury models (*13*–*18*). However, each of these methods depends on the ability of grafted cells to self-organize to form larger, organized tissue structures and leaves open the question as to the role of controlled multicellular architectural interactions during the expansion and ultimate function of grafted tissues.

Here, we fabricated a liver tissue seed that could support the in situ expansion of its cellular components in response to systemic regenerative cues after implantation in mice with liver injury. Our efforts were informed by reports of the importance of paracrine signaling between hepatocytes, endothelial cells, and stromal cells in both liver development and regeneration processes (*6*–*9*), as well as by our prior engineering efforts that demonstrated context-dependent cell signaling in microfabricated tissue microenvironments using a range of biomaterials (*2*, *19*–*23*). Our combined approach yielded an engineered, fully human tissue seed composed of human endothelial cells, hepatocytes, and fibroblasts in a degradable hydrogel that engrafted ectopically in mice and expanded more than 50-fold in situ in response to regenerative signals. The resultant human organoid phenocopied several aspects of

[1]Institute for Medical Engineering and Science, Massachusetts Institute of Technology, Cambridge, MA 02142, USA. [2]David H. Koch Institute for Integrative Cancer Research, Massachusetts Institute of Technology, Cambridge, MA 02142, USA. [3]Departments of Bioengineering and Pathology, Institute for Stem Cell and Regenerative Medicine, University of Washington, Seattle, WA 98109, USA. [4]Laboratory of Virology and Infectious Disease, Center for the Study of Hepatitis C, The Rockefeller University, New York, NY 10065, USA. [5]Department of Bioengineering, University of Pennsylvania, Philadelphia, PA 19104, USA. [6]Department of Biological Engineering, Massachusetts Institute of Technology, Cambridge, MA 02139, USA. [7]Harvard Medical School, Boston, MA 02115, USA. [8]Department of Bioengineering, Boston University, Boston, MA 02215, USA. [9]Department of Brain and Cognitive Sciences, Massachusetts Institute of Technology, Cambridge, MA 02142, USA. [10]Innolign Biomedical, Natick, MA 01760, USA. [11]Division of Gastroenterology and Hepatology, Weill Cornell Medical College, New York, NY 10065, USA. [12]Department of Electrical Engineering and Computer Science, Massachusetts Institute of Technology, Cambridge, MA 02142, USA. [13]Howard Hughes Medical Institute, Chevy Chase, MD 20815, USA.
*Corresponding author. Email: sbhatia@mit.edu

native liver structure and function, including perfused vascular networks, self-assembled structures resembling bile ducts, and production of human liver proteins secreted into mouse blood.

RESULTS

Construction of human liver tissue seeds from cellular components

We first sought to create an engineered "tissue seed" candidate by arranging a combination of human cell types in a format that would allow for expansion of the tissue seeds in situ in response to regenerative cues. Previous work had demonstrated the importance of paracrine signals between hepatocytes, endothelial cells, and stromal cells (*6*–*9*) in regeneration, as well as the requirement for defined spatial organization of engineered tissues for optimizing cellular function (*1*, *2*, *21*). We therefore incorporated human hepatocytes, endothelial cells, and stromal cells in structurally organized tissue seeds. To do this, we first used microwell technology to create aggregates of a defined size, composed of combinations of human hepatocytes and normal human dermal fibroblasts (NHDFs; Fig. 1A) (*2*). Similarly, microtissue molding was used to create patterned endothelial cord structures (*1*) from human umbilical vein endothelial cells (HUVECs) (Fig. 1B). This fabrication process was adaptable for scaled construction of larger tissues using a bioprinting process that we developed previously (fig. S1) (*4*). Finally, we coencapsulated the hepatic cellular aggregates with the endothelial cell cords in a fibrin hydrogel to create tissue seeds that were suitable for ectopic implantation in the intraperitoneal mesenteric fat of mice (Fig. 1B).

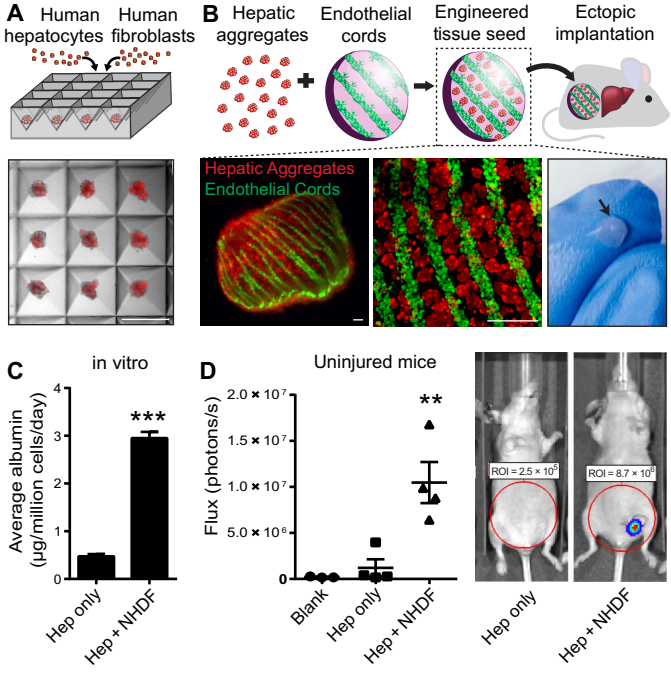

Fig. 1. Construction of human liver seed grafts. (**A**) Human hepatic aggregates containing human primary hepatocytes and NHDFs were created using pyramidal microwells. (**B**) Hepatic aggregates (red) were then combined with geometrically patterned human endothelial cell cords (green) in a fibrin hydrogel to create "liver tissue seeds" that were then implanted ectopically into FNRG mice. Right: Blue-gloved finger demonstrates macroscopic scale of human liver tissue seeds. (**C**) Human albumin production by human hepatocytes was enhanced sixfold in liver seed grafts containing both hepatocytes (Hep) and NHDFs compared to seed grafts containing only hepatocytes after culture in vitro for 6 days (***$P < 0.0001$). (**D**) Albumin promoter activity was enhanced in implanted liver seed grafts composed of human hepatocytes and NHDFs compared to those containing only human hepatocytes, 6 days after implantation into FNRG mice (**$P < 0.01$). ROI, region of interest. Scale bars, 400 μm.

As an initial characterization step, short-term in vitro tests showed that the addition of NHDFs to hepatocyte aggregates enhanced sixfold the production of human albumin, a measure of hepatic function, in a dose-dependent manner compared to aggregates containing only hepatocytes before encapsulation with endothelial cords (Fig. 1C and fig. S2). Similarly, the albumin promoter activity (*21*) of tissue seeds containing aggregates of both hepatocytes and NHDFs was enhanced more than eightfold compared to seeds containing hepatocyte-only aggregates 6 days after implantation into the mesenteric fat of healthy nude mice (Fig. 1D). Thus, the combination of human hepatocytes, endothelial cells, and stromal cells yielded candidate human liver tissue seeds that could survive engraftment in vivo.

Expansion of human hepatocytes in ectopic implants after liver injury in host mice

We hypothesized that inducing host soluble regenerative signals in mice receiving ectopic implants of liver tissue seeds might trigger these seeds to grow. Accordingly, we implanted human liver tissue seeds into the mesenteric fat of FNRG mice, an immunodeficient mouse model of the liver disease hereditary tyrosinemia type I. FNRG mice were generated by backcrossing fumarylacetoacetate hydrolase–deficient ($Fah^{-/-}$) mice with nonobese diabetic (NOD) mice, recombinase activating gene–deficient ($Rag1^{-/-}$) mice, and interleukin-2 receptor γ chain–deficient (Il2rγ-null) mice (*13*, *24*, *25*). This mouse strain experiences progressive liver failure unless treated with the small molecule 2-(2-nitro-4-fluoromethylbenzoyl)-1,3-cyclohexanedione (NTBC). NTBC was administered continuously to FNRG mice in the control group (Fig. 2A) or was given intermittently to induce cycles of liver injury and regeneration. Animals were sacrificed, and grafts were retrieved at 80 days after tissue seed implantation. Grafts were located in the mesenteric fat pad using the suture as a landmark.

To determine whether ectopic liver tissue seeds had expanded in animals in response to chronic injury and regeneration cycles induced by intermittent NTBC dosing compared to control animals, we identified human hepatocytes by immunostaining for human cytokeratin-18, an intermediate filament expressed by hepatocytes, and arginase-1, an enzyme that catalyzes the hydrolysis of arginine to ornithine and urea (*26*, *27*). Grafts from control animals treated continuously with NTBC had small cellular aggregates containing cytokeratin-18– and arginase-1–positive cells dispersed within the hydrogel (Fig. 2B, left). In animals that underwent cycles of injury and regeneration caused by intermittent treatment with NTBC, larger hepatic grafts composed of densely packed cytokeratin-18– and arginase-1–positive cells were observed (Fig. 2B, right). The cytokeratin-18–positive surface area in tissue seed grafts was quantified by a blinded observer using morphometric analysis in histologic sections. Hepatic tissue seed grafts covered significantly more surface area in FNRG animals with intermittent NTBC treatment compared to control animals (Fig. 2C, top; $P < 0.01$). Assuming that the grafts were spherical, we extrapolated graft volume on the basis of surface area measurements and calculated an average 11-fold graft expansion in NTBC-treated animals compared to control animals without liver injury (Fig. 2C, bottom; $P < 0.05$).

To assay for active proliferation in tissue seeds 80 days after implantation, we double-stained sections using antibodies against both cytokeratin-18 and Ki67, a nuclear protein associated with cellular proliferation. We identified numerous cytokeratin-18 and Ki67 double-positive cells with round nuclei characteristic of hepatocytes (Fig. 2D, left), as well as rare double-positive cells actively undergoing mitosis (Fig. 2D, right). When compared

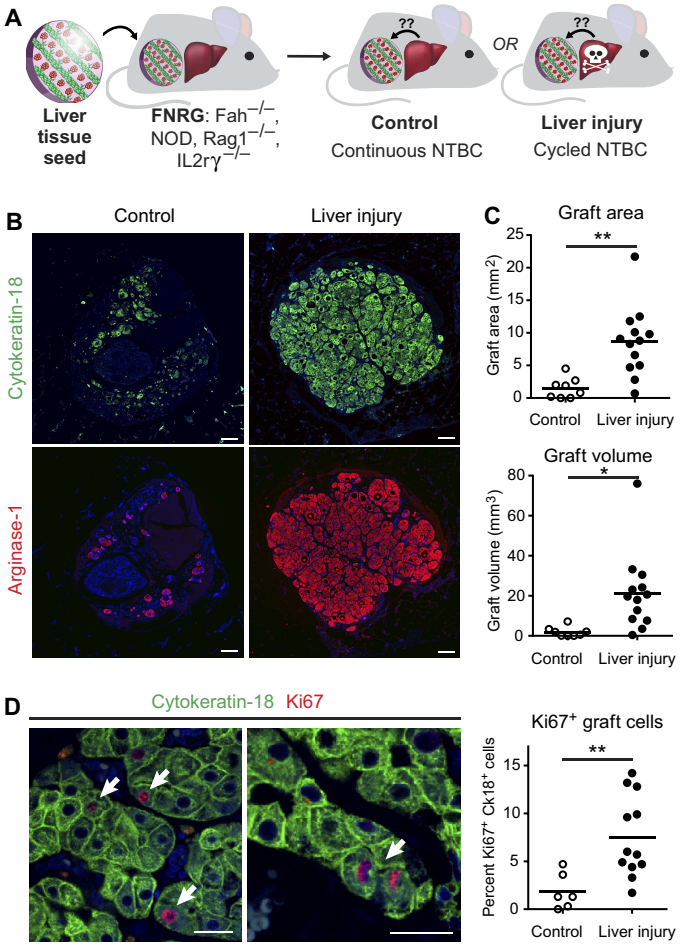

Fig. 2. Human liver tissue seed grafts expand after host liver injury. (**A**) Human liver tissue seed grafts were implanted onto the mesenteric fat of FNRG mice. The mice were treated intermittently with the small molecule NTBC to induce liver injury and regeneration or received NTBC continuously and remained injury free. (**B**) Immunostaining of liver tissue seed grafts explanted 80 days after implantation showed positive staining for the markers cytokeratin-18 and arginase-1 in animals with and without liver injury. Scale bars, 100 μm. (**C**) Histomorphometry revealed greater cytokeratin-18–positive graft area and volume in animals with liver injury compared to controls. (**D**) Many Ki67 and cytokeratin-18 double-positive cells were observed in the liver seed grafts from mice with liver injury (left, white arrows); rare Ki67 and cytokeratin-18 double-positive cells undergoing mitosis were also observed (right, white arrows). Graph shows that liver seed grafts in animals with liver injury exhibited a greater number of Ki67 and cytokeratin-18 double-positive cells compared to uninjured animals. Scale bars, 10 μm. *$P < 0.05$, **$P < 0.01$ (Student's t test).

with control animals, fourfold more cytokeratin-18 and Ki67 double-positive cells were observed in grafts from animals that received cycles of NTBC to induce liver injury and regeneration (Fig. 2D, graph; $P < 0.01$).

To test whether our candidate tissue seeds also responded to regenerative cues after acute liver injury, we implanted seed grafts into the mesenteric fat of athymic mice. After a 1-week engraftment period, mice were subjected to two-thirds partial hepatectomy of the host liver to promote liver regeneration and given 5-ethynyl-2′-deoxyuridine (EdU) every 12 hours to label cells in the S phase of the cell cycle. One week after hepatectomy, animals were sacrificed, and engrafted tissues were excised, sectioned, and double-immunostained using antibodies that recognized EdU and cytokeratin-18 to identify hepatocytes in the S phase of the cell cycle. Grafts subjected to regenerative signals induced by hepatectomy injury contained more EdU and cytokeratin-18 double-positive cells compared to controls (fig. S3).

Hepatic function of ectopic liver seed grafts

To evaluate the functional characteristics of the expanded hepatic seed grafts, we studied two major axes of liver function: synthesis and drug metabolism, and also performed a more global analysis of liver seed graft phenotypes. We first measured the protein synthesis capacity of the grafts by testing for human proteins in mouse serum. We detected human albumin in serum from engrafted mice treated with NTBC as early as day 3; the concentration of human albumin increased 50-fold from day 3 to the end point of the experiment in the NTBC-treated animals (Fig. 3, A and B). The maximum human albumin concentration detected in a single animal undergoing cycles of liver injury and regeneration was 105 μg/ml. Human serum albumin concentrations began to diverge between the treatment groups at about day 20, and liver seed grafts in animals with liver injury produced more albumin than those in control animals (Fig. 3, A and B; 10-fold difference at the end point of the experiment; $P < 0.001$). In addition to human albumin, blood drawn from NTBC-treated animals showed increased concentrations of human transferrin, α1-antitrypsin, and fibronectin relative to controls (Fig. 3C; $P < 0.05$). These results suggested that human hepatocytes in ectopic tissue seed grafts were functional and synthesized more human proteins when in the presence of regenerative signals induced by liver injury, compared to uninjured control animals.

To gauge the potential utility of liver seed grafts for studies of drug metabolism, we characterized the expression and induction of human drug-metabolizing enzymes and other key liver-specific proteins in expanded grafts implanted into FNRG mice. We first collected RNA for RNA sequencing (RNA-seq) analysis from liver seed grafts explanted from injured host mice, as well as from control samples comprising healthy human liver, primary human hepatocytes, HUVECs, and NHDFs. We then looked at the expression of 50 genes representing different hepatic gene classes that were expressed in both control human liver and primary human hepatocyte RNA samples. These gene groups included CYP3A4 and CYP2B6 for cytochrome P450 activity, SULT1A1/2A1 for sulfotransferase activity, SLCO1A2/1B1 for anion transporter activity, ABCB/ABCG for adenosine 5′-triphosphate (ATP)–binding transporters, APOB/APOE for lipoprotein biosynthesis, albumin for biosynthesis, and HNF4A/G encoding key transcription factors. Read counts across groups were normalized to human primary hepatocyte control RNA samples to create an expression heat map (Fig. 3D). A total of 47 of 50 of these liver-specific genes were expressed in explanted liver seed grafts, compared to 18 of 50 genes expressed in unexpanded HUVEC and NHDF RNA samples. Genes from each of the major hepatic drug metabolism pathways were expressed in liver seed grafts at similar levels to the human liver, including cytochrome P450 enzymes (Fig. 3E), sulfotransferases (Fig. 3F), and anion transporters and ATP-binding transporters (Fig. 3, G and H). In addition to hepatic gene expression studies, we tested the ability of liver seed grafts to up-regulate key drug metabolism enzymes in response to a known human CYP450 inducer (*21*). We administered rifampin or vehicle control to FNRG animals treated with NTBC bearing expanded liver seed grafts, euthanized the animals, and collected RNA from explanted liver seed grafts. We found that rifampin induced CYP3A4 expression in liver seed grafts, a highly liver-specific phenomenon indicative of mature hepatocyte function (Fig. 3I).

Finally, we sought to interrogate the transcriptional profile of liver seed grafts more globally. We first used Ingenuity Pathway Analysis to assess the fraction of genes known to be downstream of given transcription factors that were differentially regulated between

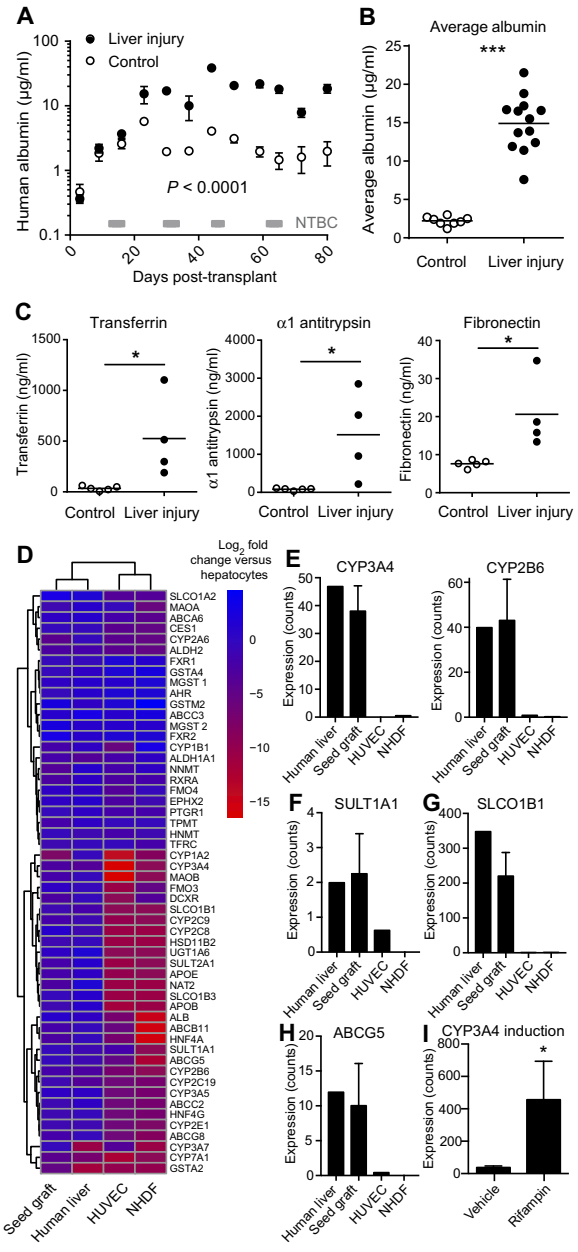

Fig. 3. Human liver tissue seed graft function. Mice were implanted with liver seed grafts, and the host mice were treated intermittently with NTBC to induce liver injury and repair (14 days off, followed by 3 to 4 days on; gray bars). (**A**) Blood samples were collected weekly by retro-orbital bleeding. The concentration of human albumin in mouse serum was greater in animals with liver injury compared to controls [$P < 0.0001$, one-way analysis of variance (ANOVA)]. (**B**) Human albumin concentration for each animal averaged across all time points. (**C**) The concentrations of human transferrin, α1-antitrypsin, and fibronectin in mouse serum were greater in animals receiving intermittent NTBC treatment (liver injury) compared to controls at 80 days after implantation into FNRG mice. (**D**) mRNA expression analysis of explanted liver seed grafts demonstrated that 47 of 50 liver-specific genes were expressed in explanted liver seed grafts (denoted "Seed graft") compared to 18 of 50 human genes expressed in HUVEC and NHDF cell lines. (**E** and **F**) Genes from each of the major hepatic drug metabolism pathways were expressed in liver seed grafts at levels similar to those of the human liver. (**G** and **H**) Mice with liver seed grafts were injected with rifampin solution (25 mg/kg, intraperitoneally) or vehicle control daily for 3 days and, again, 1 hour before sacrifice. (**I**) Rifampin induced greater CYP3A4 expression in expanded liver seed grafts compared to mice injected with vehicle control. *$P < 0.05$, ***$P < 0.001$ (Student's t test).

expanded liver seed grafts and HUVEC or NHDF control cells. This analysis identified distinct transcriptional regulation in liver seed grafts by hepatocyte transcription factors in the HNF1, HNF3, and HNF4 families, as well as C/EBP (CCAAT/enhancer-binding protein), compared to HUVEC or NHDF control cells (fig. S4A). This suggested that the hepatocytes present in expanded liver seed grafts displayed a lineage-appropriate phenotype. Furthermore, given that liver seed grafts were composed of primary hepatocytes, HUVECs, and NHDFs, we sought to test whether expression profiles from each of these three cell types were detectable in liver seed grafts after expansion. Hierarchical clustering of expression RNA-seq profiles obtained from samples of expanded liver seed grafts, pure human primary hepatocytes, human liver tissue, and pure populations of cultured NHDFs and HUVECs demonstrated that RNA expression in liver seed grafts clustered between those of primary hepatocytes/human liver samples and those of nonparenchymal HUVEC and NHDF cell lines. This was consistent with an intermediate phenotype driven by the presence of each of these three cell types within the expanded graft (fig. S4B).

Characterization of liver seed graft morphology after transplant

Our earlier-generation engineered tissues, when implanted into uninjured mouse hosts, were characterized histologically by the presence of disperse hepatic aggregates within fibrin hydrogels upon explant (*1*, *2*, *21*). Here, we hypothesized that cells would self-organize in response to regenerative stimuli as the tissue seeds expanded. Immunohistological characterization revealed that the expanded liver seed grafts in NTBC-treated FNRG mice contained densely packed polyhedral cells resembling hepatocytes, many of which were binucleated (Fig. 4A; staining with hematoxylin and eosin). These cells stained positively for the hepatocyte markers cytokeratin-18 and arginase-1 (Fig. 4, B and C). Hepatocytes in expanded liver seed grafts were organized into dense aggregate-like units that, in some cases, exhibited structures reminiscent of hepatic cords in the normal human liver (Fig. 4B). Furthermore, hepatic units in expanded liver seed grafts were arranged within a syncytium of interconnected lacunae containing endovascular stroma and lined with collagen III, which lines hepatic cords in the space of Disse in the human liver (Fig. 4D, staining for reticulin). In addition, liver seed grafts were examined for the expression of multidrug resistance–associated protein 2 (MRP2; also known as ABCC2), which is selectively transported to the apical (that is, canalicular) domain of hepatocytes in the human liver. We observed that hepatocytes in expanded liver seed grafts exhibited polarized expression of MRP2 (Fig. 4C). Tissue seed grafts also contained bile canalicular–like structures between adjacent hepatocytes characteristic of normal liver structure (Fig. 4C), as well as larger vacuolar structures expressing MRP2 (Fig. 4C).

Further characterization with hematoxylin and eosin staining revealed that expanded tissue seed grafts also contained duct-like structures resembling bile ducts (Fig. 4E, arrows). To further examine whether biliary epithelial–like cells were present in ectopic grafted tissues, we immunohistochemically stained tissue sections for expression of both cytokeratin-18 (a cytokeratin expressed by hepatocytes and biliary epithelial cells) and cytokeratin-19 (a cytokeratin expressed by biliary epithelial cells but not hepatocytes). Cells organized in ductal structures stained positively for both cytokeratin-18 and cytokeratin-19, suggesting that these cells exhibited biliary epithelial–like characteristics (Fig. 4F). Notably, cytokeratin-18 and cytokeratin-19 double-positive ductal structures were typically located within connective tissue and adjacent to human CD31–positive blood vessels, many of which contained Ter-119–positive erythroid cells (Fig. 4F). To further confirm both the

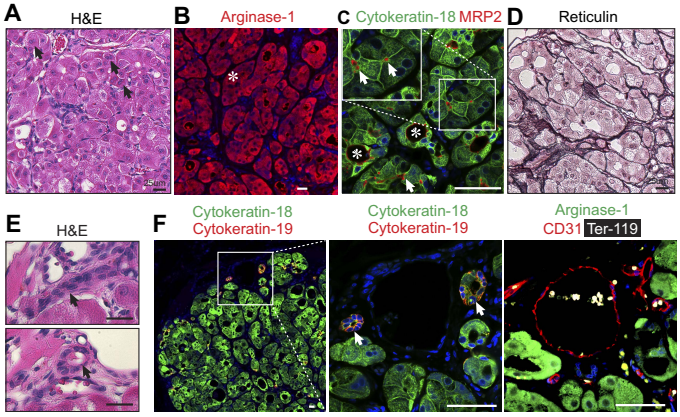

Fig. 4. Characterization of human liver seed graft morphology. (**A**) Immunohistochemical staining of human liver tissue seed grafts from animals with liver injury sacrificed at day 80 revealed densely packed polyhedral cells resembling hepatocytes [stained with hematoxylin and eosin (H&E)] that were positive for both arginase-1 (**B**) and cytokeratin-18 (**C**). These human hepatocytes sometimes self-organized into cord-like structures (white star) (B). Hepatocytes were polarized, forming MRP2-positive bile canalicular–like structures between hepatocytes (white arrows, inset) and larger vacuoles lined with MRP2 (white stars) (C). (**D**) Hepatic units within the human liver seed grafts were surrounded by a syncytium of interconnected lacunae lined with collagen III as indicated by reticulin staining. (**E**) Human liver tissue seed graft sections stained with hematoxylin and eosin contained duct-like structures that resembled bile ducts (black arrows). (**F**) Cells in the ductal structures present in expanded liver seed grafts stained positive for cytokeratin-19, which is a marker for biliary epithelial cells but does not stain human hepatocytes (left). Cells organized in ductal structures stained positively for both cytokeratin-18 and cytokeratin-19 (white arrows, inset) (middle). Ductal structures were typically located adjacent to blood vessels lined with human CD31–positive endothelial cells and containing Ter-119–positive red blood cells (right). Scale bars, 25 μm.

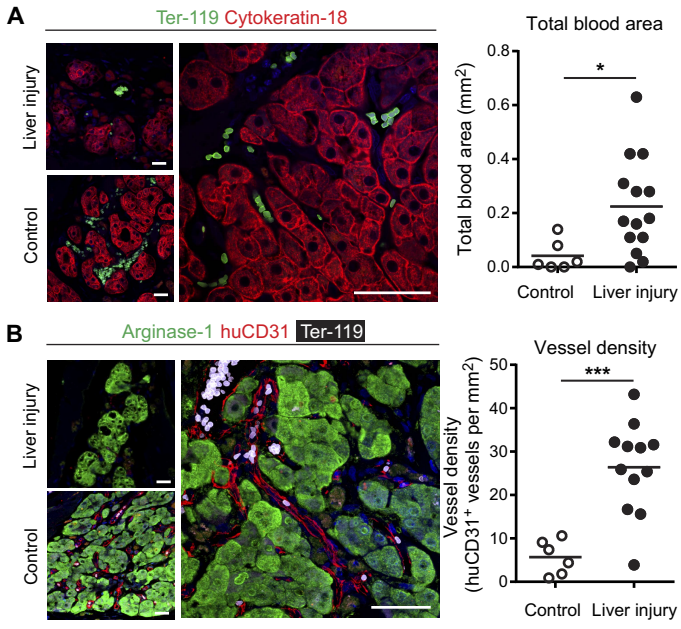

Fig. 5. Vascularization of human liver seed grafts. (**A**) Lacunae between hepatocytes (red) contained Ter-119–positive red blood cells in liver seed grafts in animals with liver injury (left, green). Graph shows that liver seed grafts in animals with NTBC-induced liver injury and regeneration contained a greater number of red blood cells than did those in control animals. (**B**) Blood vessels containing Ter-119–positive red blood cells (white) and lined in part by human endothelial cells (red) were identified in tissue seed grafts (left). Liver seed grafts from animals with liver injury contained more human CD31 (huCD31)–positive blood vessels compared to grafts in control mice (right). Scale bars, 25 μm. *P < 0.05, ***P < 0.001 (Student's t test).

biliary epithelial cell–like phenotype and whether these cells were of human origin, we stained tissue sections for human cytokeratin-18 and a second cytokeratin expressed on biliary epithelial cells but not hepatocytes, human cytokeratin-7. Ungrafted mouse control liver tissue did not stain with either human marker, whereas positive control human liver tissue contained cytokeratin-18 and cytokeratin-7 double-positive cells in ductal structures (fig. S5). Ductal structures in ectopic liver seed grafts stained positive for both cytokeratin-18 and cytokeratin-7, further confirming that they were composed of human cells with an epithelial cell phenotype (fig. S5). We hypothesized that biliary epithelial–like cells identified in liver seed grafts may have arisen at least partially from contaminating biliary epithelial cells present in cryopreserved human hepatocyte samples. To test this hypothesis, we immunostained for cytokeratin-19 expression using cells from primary hepatocyte samples immediately upon thawing. We identified cytokeratin-19–positive cells in both of the human hepatocyte primary cell samples used in this study (0.16 and 0.13% of total cells in hu8085 and NON sample lots, respectively; fig. S6), suggesting that self-assembling biliary-like structures may have been at least partially derived from these cells. These results suggested that human biliary epithelial–like cells self-assembled to form ductal-like structures at an ectopic location within human liver tissue seeds and that these ductal structures were associated with other classic features of portal triads, such as vasculature and connective tissue.

Concomitant expansion of blood vessels lined with human endothelial cells

Given that lacunae in the human liver form the vascular sinusoidal network that feeds hepatocytes with blood, we wondered whether interconnected lacunae observed in hepatic liver seed grafts contained red blood cells and whether regenerative cues would promote expansion of the total blood in the liver seed graft. We observed numerous cells resembling red blood cells in the lacunae of expanded seed grafts by hematoxylin and eosin staining (Fig. 4A). We further confirmed the identity of such cells by staining for Ter-119, an erythrocyte marker (Fig. 5A). We also quantified total blood area and observed that liver seed grafts from animals subjected to cycles of liver injury and regeneration contained significantly more red blood cells compared to those from control animals (Fig. 5A; $P < 0.05$), suggesting that the blood pool coordinately expanded with the expansion of hepatic seed grafts in animals with liver injury.

The presence of red blood cells in expanded tissue seed grafts suggested that vascular networks might be present in these grafts. Furthermore, several existing ectopic engraftment models have been shown to recruit host-derived vascular components, and human hepatocytes and vascular cells are known to expand in concert during liver regeneration (*6*, *28*, *29*). These observations led us to hypothesize that the prepatterned human endothelial cells within hepatic seed grafts may also expand in response to regenerative cues after liver injury. Thus, we immunostained expanded liver seed graft sections with antibodies recognizing human CD31 (endothelial cells), Ter-119, and arginase-1. Vessels lined in part by human endothelial cells were identified throughout the liver seed grafts that had expanded in FNRG mice treated with cycles of NTBC (Fig. 5B). Incubation of explanted graft sections in a solution containing lectins that bound specifically to human or mouse endothelium demonstrated that vessels were lined with both human and mouse endothelial cells (fig. S7). Many of these vessels contained Ter-119–positive erythroid

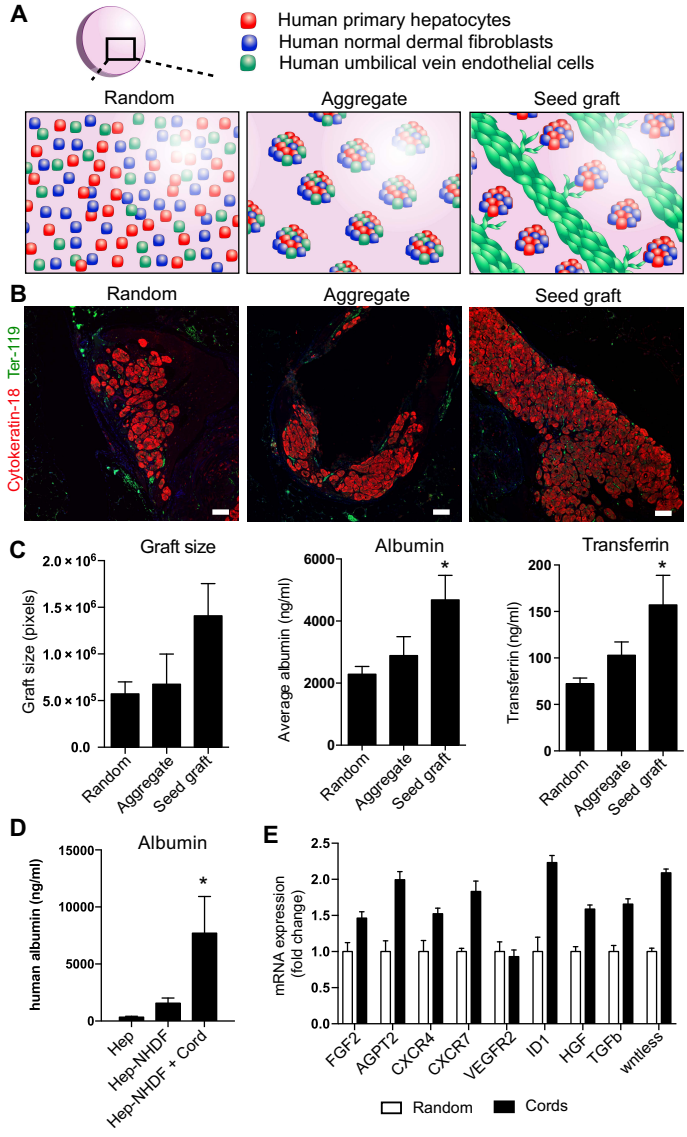

Fig. 6. Tissue architecture affects function of expanded liver seed grafts. (**A**) Human liver tissue seed grafts were created in three different constructs: (left) human hepatocytes, HUVECs, and NHDFs randomly organized as single cells within a fibrin hydrogel; (middle) human hepatocytes, HUVECs, and NHDFs in tri-cell aggregates randomly seeded in a fibrin hydrogel; and (right) human hepatocytes and NHDFs in aggregates, and HUVECs in endothelial cords, then combined in a fibrin hydrogel. (**B**) All three architectural conformations produced cytokeratin-18 –positive hepatic grafts after expansion in response to liver injury. Scale bars, 100 μm. (**C**) Graft size, as measured by histomorphometry, was not different between the three constructs. Hepatic function, as measured by human albumin and transferrin production, was increased in the original liver seed grafts. (**D**) Inclusion of both NHDFs and HUVECs in the liver seed grafts was necessary for maximal hepatic function after expansion in response to liver injury. (**E**) A comparison of the gene expression patterns in endothelial cell constructs with either random HUVECs or endothelial cell cords, 1 day after formation of the tissues in vitro, revealed that preorganization of HUVECs into endothelial cell cords resulted in increased expression of several key endothelial genes. *$P < 0.05$, one-way ANOVA.

cells (Fig. 5B). Blood vessels lined with CD31-positive human endothelial cells were located in the lacunae between and within hepatic units (Fig. 5B). Liver seed grafts in mouse hosts with liver injury showed more vessels containing human endothelial cells compared to liver seed grafts in control animals (Fig. 5B; $P < 0.01$). Ki67-positive human endothelial cells were present but were rare (less than one Ki67-positive and human CD31–positive cell per 1-mm section of liver seed graft). This suggested that most endothelial cells were not undergoing active cell cycle progression at the time of graft explant (fig. S8).

Impact of liver seed graft architecture on expansion after liver injury

Given that tissue architecture ultimately defines the cell-cell contacts and paracrine signaling gradients that drive cellular phenotype and function, we hypothesized that the initial cell position in liver seed grafts would affect expansion in response to regenerative stimuli after liver injury. We created three constructs using varying arrangements of human hepatocytes, human endothelial cells, and human stromal cells. Three configurations were tested, including (i) the three cell types randomly organized as single cells within a fibrin hydrogel, (ii) the three cell types forming tri-cell aggregates and suspended randomly within a fibrin hydrogel, and (iii) the original liver seed graft architecture in which hepatocytes and stromal cells were patterned in aggregates and embedded in the fibrin hydrogel alongside organized endothelial cell cords (Fig. 6A). Constructs were implanted in the mesenteric fat of FNRG mice, and the small molecule NTBC was administered intermittently to induce cycles of liver damage and regeneration in all groups. The size of cytokeratin-18–positive hepatic seed grafts after explant appeared to increase more in animals with the original liver seed grafts, but this difference did not reach significance (Fig. 6, B and C). Nonetheless, concentrations of human albumin and transferrin in mouse serum were greater in mice receiving the original liver seed graft than those receiving the other two constructs (Fig. 6C). To further assess the relative importance of the inclusion of different cell types in mediating liver seed graft expansion, we next removed NHDFs or endothelial cell cords from liver seed grafts before implanting into FNRG mice and initiating liver injury. We found that each cellular element in the liver seed grafts had a positive impact on the production of human albumin, and this effect reached significance in the presence of all three cell types (Fig. 6D; $P < 0.05$).

Finally, we sought to explore the mechanism by which cell patterning might play a role in tissue expansion. We created tissues containing either randomly organized endothelial cells or endothelial cells patterned into cords. We then analyzed the expression of key genes known to be up-regulated in endothelial cells and to enhance hepatocyte proliferation during liver regeneration (*6*, *29*). We found that expression of mRNAs for multiple factors was up-regulated in patterned endothelial cell cords versus randomly organized endothelial cells (Fig. 6E).

DISCUSSION

Here, we explore the concept of constructing a seed of liver tissue from mature human cell populations that coordinately grows after implantation into mice. We have called these liver seed grafts SEEDs for "In Situ Expansion of Engineered Devices." These liver seed grafts were composed of human parenchymal cells, vascular cells, and stromal cells arranged in a specified architecture in a degradable fibrin hydrogel that collectively favored self-organized expansion in response to regenerative stimuli after liver injury. We have shown that these hepatic SEEDs can engraft and expand ectopically by 50-fold over time and demonstrated the emergence of self-organized biliary epithelial structures within the newly formed, vascularized hepatic parenchyma.

The composition of our tissue seeds was influenced by previous work in both biology and engineering that probed the multicellular

paracrine signaling loops that exist between hepatocytes, endothelial cells, and stromal cells. For example, hepatocyte growth factor, transforming growth factor–α, Wnt2, and angiopoietin-2 communicate signals from stellate cells or endothelial cells to neighboring hepatocytes that are known to be critical for normal organogenesis and regeneration (*6*, *28*–*30*). Given that paracrine signals are influenced by the spatial proximity between different cell types, engineers have further developed microfabrication technologies to better understand how microstructural arrangements of cells within the tissue affect tissue signaling and function. In the case of the liver, such studies have shown that culturing hepatocytes in spheroids or aggregates with other hepatocytes (*2*, *21*), stromal cells in direct contact with hepatocytes (*2*, *21*, *23*), and endothelial cells near to but not in contact with hepatocytes (*2*, *21*) leads to optimal hepatic function in engineered platforms. For fabricating the liver tissue seeds used in this study, the goal was not to mimic the structure of the tissue but rather to specify an engineered environment that could stabilize parenchymal function and direct in situ cellular expansion in response to systemic regenerative cues after implantation into mice with liver injury. We used our architectural patterning capabilities to create human hepatic tissues with varying cellular patterning conformations and then probed whether the structural architecture affected the ultimate function of the expanded liver tissue seed grafts. Our results demonstrated that patterning stromal cells in immediate proximity to hepatocytes within cellular aggregates, and including distinct endothelial cords near to but not touching hepatic aggregates in the fibrin hydrogel, resulted in liver seed grafts with increased function after expansion compared to alternative cell arrangements.

In addition to local signals from neighboring cell types, our liver seed grafts responded to systemic regenerative signals after liver injury in mouse hosts. A systemic effect of liver injury on a distant uninjured organ was first described by parabiosis studies linking the circulation of two animals (*31*) and more recently in studies grafting hepatocytes ectopically into the lymph nodes and other locations of mice (*18*, *32*–*34*). Expansion of primary adult human hepatocytes in our studies demonstrated that signals generated in the mouse in response to two forms of regeneration-inducing injury could result in human tissue seed growth, suggesting that at least some relevant mouse growth factors can cross-react with cognate receptors on human cells. The signals mediating this interaction likely include growth factors known to control hepatocyte proliferation during regeneration and development, such as hepatocyte growth factor (*9*, *35*, *36*). Next-generation markers (*37*) might further enable elucidation of regenerative cues elicited by liver cirrhosis and other liver diseases. If regenerative cues in human disease are insufficient to induce robust expansion of the hepatic seed grafts developed here, additional microenvironmental cues such as microbeads releasing small molecules or growth factors might be incorporated to trigger hepatocyte proliferation and expansion (*38*, *39*).

Notably, ectopic liver tissue seed grafts in our studies also contained biliary epithelial–like cells that frequently self-organized into structures resembling bile ducts. The origin of these structures remains an open question. Whereas rare biliary lineage cells were present in the human primary hepatocyte isolates, there have also been recent documentations of adult human hepatocytes giving rise to this lineage during liver injury in other systems (*40*, *41*). Our observation of biliary duct–like structures in ectopic liver tissue grafts thus requires additional characterization but nonetheless represents an important first step toward creating ectopic human livers with hallmark anatomic features of the native organ.

To date, most cell-based strategies for treating liver diseases have involved direct engraftment of hepatocytes into the host liver (*42*). The efficacy of this approach is likely to be limited in most of the patients with end-stage liver disease because cirrhosis and fibrosis limit cellular engraftment. We and others (*18*, *32*–*34*, *43*, *44*) are pursuing the development of a therapeutic satellite liver that could be implanted in an ectopic location in a patient and provide functional support to the failing liver. Although human induced pluripotent stem cell (iPSC)–derived hepatocyte-like cells have been engrafted ectopically in a prior study (*45*), iPSC-derived cell therapies must still address a variety of concerns, including challenges in creating mature cell populations that exhibit robust adult functions, the potential for teratoma formation, and the time needed for cellular expansion and differentiation. The present study represents a complementary approach, in which we use regenerative cues after injury to the mouse liver to stimulate the expansion of an ectopic adult human tissue. The current study sheds light on the importance of refined construct engineering in enabling expansion of adult human hepatocytes.

We believe that this work sets the stage for using SEEDs as an alternative strategy for scale-up of engineered organs, one that uses native developmental, injury, or regenerative signals to expand prefabricated constructs in situ. However, more work must be done before liver seed grafts are ready for the clinic. First, although our studies demonstrated that expanded liver seed grafts exhibited several adult hepatic functions, additional studies must be performed to further analyze the capability of these seed grafts to recapitulate the more than 500 functions of the adult human liver (for example, production of human-specific drug metabolites and further analysis of biliary function). Second, although liver seed graft expansion was augmented using engineering tools such as geometric patterning and material cues in this study, expansion may be further supported by inclusion of additional microenvironmental factors, such as controlled delivery of mitogens (*12*, *46*). Third, to attain the ~10 billion human hepatocytes necessary to treat several forms of liver disease, liver seed grafts will need to be further scaled up in size, likely in combination with other technologies. One could envision bioprinting of tissue seeds followed by postimplantation expansion as an alternative to printing a whole human organ in vitro. Finally, future studies should be undertaken to determine whether liver seed grafts could be useful in other forms of liver injury, such as cirrhosis.

MATERIALS AND METHODS

Study design

Sample size justification for all studies was performed using power analysis. We used $n = 3$ to 4 cell cultures per group for in vitro experiments and $n = 6$ to 9 animals per group for in vivo experiments. The overall objective of this study was to test whether engineered human liver seed grafts that were implanted ectopically in host mice expanded and became functional in response to regenerative signals after liver injury. In vivo studies generally included two groups of mice. All mice were implanted with liver seed graft constructs and then were randomly divided into one of two groups: One group sustained liver injury, and the other control group did not. End points were designed to assess hepatocyte phenotype and function on the basis of a variety of established assays. All histomorphometric analyses were performed by a blinded observer. Studies were repeated at least three times.

Cell culture

Primary cryopreserved human hepatocytes (Lot NON, 35-year-old, Caucasian, female from Celsis or Lot hu8085 1-year-old, female, Caucasian from Invitrogen) were maintained in high-glucose Dulbecco's

modified Eagle's medium (DMEM) (CellGro) containing 10% (v/v) fetal bovine serum (FBS) (Gibco), 1% (v/v) ITS supplement (insulin, transferrin, sodium selenite; BD Biosciences), glucagon (0.49 pg/ml), dexamethasone (0.08 ng/ml), 0.018 M Hepes, and 1% (v/v) penicillin-streptomycin (Invitrogen). Primary HUVECs (Lonza; passages 4 to 7) were maintained in dishes in EGM-2 media (Lonza). NHDFs (Lonza; passages 4 to 8) were cultured in DMEM with 10% (v/v) FBS and 1% (v/v) penicillin-streptomycin.

Fabrication of micropatterned tissue seeds

Engineered liver tissue seeds were fabricated using previously described methods (*1*). To create hepatic aggregates, human primary hepatocytes were thawed and immediately plated into AggreWell micromolds along with NHDFs and incubated overnight. To create endothelial cords, HUVECs were suspended at a density of 3 million HUVECs/ml liquid collagen (2.5 mg/ml) (BD Biosciences) and centrifuged into polydimethylsiloxane channels. Collagen was polymerized, and constructs were incubated in EGM-2 media for 4 hours to allow for cord formation. Endothelial cord arrays were then embedded in fibrin (10 mg/ml) (human thrombin, Sigma-Aldrich; bovine fibrinogen, Sigma-Aldrich). Hepatic aggregates (about 100 hepatocytes and 200 dermal fibroblasts per aggregate) were suspended in fibrin (10 mg/ml) at a concentration of 90,000 aggregates/ml fibrin and added in a second layer over endothelial cords to encase the cords in hepatic aggregates and fibrin gel. Synthetic tissues were cut with a 6-mm biopsy punch immediately before implantation. Each seed tissue contained about 150,000 human hepatocytes, 300,000 dermal fibroblasts, and 150,000 HUVECs upon implantation.

For bioprinted constructs (fig. S1), sacrificial lattices of carbohydrate glass were constructed using a custom-built three-dimensional printer containing a heated nozzle as described previously (fig. S1, left) (*4*), embedded within a fibrin hydrogel, and dissolved using phosphate-buffered saline (PBS) to leave open channels (fig. S1, middle). Channels were filled by pipetting a slurry containing HUVECs and neutralized collagen using methods and cell densities described above.

Implantation and induction of liver injury

All surgical procedures were conducted according to protocols approved by The Rockefeller University and the Massachusetts Institute of Technology institutional animal care and use committees. Eight- to 12-week-old female NCr nude (Taconic; for uninjured mouse studies in Fig. 1 and partial hepatectomy studies in fig. S3.) or Fah$^{-/-}$ backcrossed to NOD, Rag1$^{-/-}$, and Il2rγ-null (FNRG) mice (Yecuris) (*13*, *24*, *25*) were anesthetized using isoflurane, and the synthetic tissue constructs were sutured to the mesenteric parametrial fat pad (one tissue per animal for nude mouse studies and four tissues per animal for FNRG studies). The incisions were closed aseptically, and the animals were administered buprenorphine (0.1 mg/ml) every 12 hours for 3 days after surgery. NTBC was withdrawn from animals' drinking water immediately after synthetic tissue implantation and for 14 days after implantation. NTBC was then administered for 4 days and then cycled off/on in 14 days off and 3 to 4 days on increments for the remainder of the experiment.

For hepatectomy studies, partial hepatectomy liver injury was performed 1 week after implantation of SEEDs. Before hepatectomy surgery, mice were administered carprofen (5 mg/kg, subcutaneously). Partial hepatectomy was then performed as described previously (*47*), with slight modifications. Specifically, the left lateral and left median lobes were excised, sparing the gall bladder. The abdomen was washed with saline before closing the peritoneum with Vicryl sutures. After hepatectomy, animals were injected with EdU (50 mg/kg) (Thermo Fisher Scientific) daily until sacrifice at 7 days after hepatectomy.

Bioluminescence imaging

To enable noninvasive imaging of the survival of functional hepatocytes, primary human hepatocytes were transduced in suspension culture immediately upon thawing with a lentiviral vector expressing firefly luciferase under the human albumin promoter (pTRIP.Alb.IVSb.IRES.tagRFP-DEST, gift of C. Rice, The Rockefeller University) before liver tissue seed fabrication. For viral transduction, concentrated virus was diluted 1:5 into a hepatocyte medium containing Hepes buffer (20 mM; Invitrogen) and polybrene (4 μg/ml; Invitrogen) in six-well ultralow attachment plates (Corning). Immediately before bioluminescence imaging, mice were injected intraperitoneally with 250 μl of D-luciferin (15 mg/ml; Caliper Life Sciences) and imaged using the IVIS Spectrum (Xenogen) system and Living Image software (Caliper Life Sciences).

Biochemical assays

Throughout the experiment, mice were bled retro-orbitally, blood was collected, and serum was separated by centrifugation. Serum levels of human albumin were determined by an enzyme-linked immunosorbent assay (ELISA) using goat polyclonal capture and horseradish peroxidase–conjugated goat anti-human albumin detection antibodies (Bethyl Laboratories). At the time of sacrifice for some animals, blood was retrieved via cardiac puncture and collected in clot-activating tubes. Serum levels of human albumin (Bethyl), human α1-antitrypsin (Bethyl), and human fibronectin (Boster) were determined by ELISA.

Tissue harvesting and immunohistochemistry

Animals were sacrificed at the termination of the experiment (80 to 84 days). Tissue was harvested from the intraperitoneal space, and explants were fixed in 4% (v/v) paraformaldehyde for 48 hours at 4°C. Explants were sectioned into about 1-mm sections by hand and then dehydrated in graded ethanol (50 to 100%), embedded in paraffin, and sectioned using a microtome (6 μm) for immunohistochemical staining. All morphometric analyses (for example, graft size) were performed on stained 6-μm sections from the surface of all 1-mm sections of each graft.

For gross visualization of tissue, sections were stained with hematoxylin and eosin. For visualization of type III collagen, sections were stained with reticulin/nuclear fast red stain (Dako). For identification of primary human hepatocytes, sections were incubated with primary antibodies against human cytokeratin-18 (mouse, 1:25; Dako) or arginase-1 (rabbit, 1:400; Sigma-Aldrich) and followed with species-appropriate secondary antibodies conjugated to Alexa Fluor 647. To determine graft size, we used Adobe Photoshop to quantify the number of cytokeratin-18–positive pixels in each graft. For identification of primary human hepatocytes in active cell cycle phases, sections were blocked using M.O.M. Blocking Reagent (Vector Laboratories) and normal donkey serum, then incubated with primary antibodies against human cytokeratin-18 (mouse, 1:25; Dako) and Ki67 (rabbit, 1:500; Abcam), and followed with species-appropriate secondary antibodies conjugated to Alexa Fluor 555 and 647.

For identification of primary human hepatocytes and human bile canaliculi, sections were blocked using M.O.M. Blocking Reagent and normal donkey serum, then incubated with primary antibodies against human cytokeratin-18 and human MRP2 (rabbit, 1:100; Abcam), and followed with species-appropriate secondary antibodies conjugated to Alexa Fluor 555 and 647. For identification of primary hepatocytes, human endothelial cells, and mouse red blood cells, sections were first blocked using M.O.M. Blocking Reagent and normal donkey serum

and then immunostained using primary antibodies against human arginase-1 (rabbit, 1:400; Sigma-Aldrich), human CD31 (mouse, 1:20; Dako), and Ter-119 (rat, 1:100; BD Pharmingen), respectively. Signal was visualized after incubation with secondary goat anti-mouse–Alexa Fluor 555, donkey anti-rat–Alexa Fluor 488, and donkey anti-rabbit–Alexa Fluor 647 antibodies (Jackson ImmunoResearch). For identification of primary human hepatocytes and biliary cells, sections were blocked using M.O.M. Block Reagent and normal donkey serum, then immunostained with primary antibodies against human cytokeratin-18 and cytokeratin-19 (rabbit, 1:250; Abcam) or human cytokeratin-7 (rabbit, 1:300; Novus), and followed with species-appropriate secondary antibodies conjugated to Alexa Fluor 555 and 647. Positive control human adult liver sections were purchased from Abcam. For identification of biliary cells in human hepatocyte cell lots, 50,000 freshly thawed cells from each human hepatocyte lot were deposited on glass slides using a Cytospin Cytocentrifuge and then immunostained for cytokeratin-19, as described above. Images were obtained using a Nikon Eclipse Ti microscope, Nikon 1AR ultrafast spectral scanning confocal microscope, or Zeiss AxioCam HRm stereoscope.

For SWITCH (system-wide control of interaction time and kinetics of chemicals) tissue clarification, 1-mm-thick sections of explanted expanded liver seed grafts were treated with glutaraldehyde and then cleared with 200 mM SDS using methods we developed previously (*48*). To visualize mouse versus human vessels, cleared expanded liver seed graft sections were incubated in a solution of lectin (500 μg/ml) from *Helix pomatia* agglutinin (HPA) conjugated to Alexa Fluor 488 (Sigma-Aldrich) and lectin (100 μg/ml) from *Ulex europaeus* agglutinin–1 (UEA-1) conjugated to tetramethyl rhodamine isothiocyanate (Vector Laboratories) in PBS, which have been shown previously to bind to mouse or human endothelial cells, respectively (*1*). Images were obtained using an Olympus 10× CLARITY immersion medium 0.6–numerical aperture objective.

RNA-seq and bioinformatics

Total RNA was extracted from explanted liver tissue seed grafts ($n = 3$), primary cryopreserved human hepatocytes (immediately after thawing; $n = 2$), human liver ($n = 1$), HUVECs ($n = 1$), and NHDFs ($n = 1$) using Qiagen RNeasy Mini Kits. RNA was passed through initial quality control using an Agilent bioanalyzer, polyadenylate-purified and converted to complementary DNA using the Illumina TruSeq protocol, run on SPRIworks System (Beckman Coulter) using custom barcodes for library preparation, enriched by polymerase chain reaction, and submitted for Illumina sequencing. Forty-nucleotide paired-end sequencing was then performed on an Illumina HiSeq 2000. A standard pipeline was used for quality control of HiSeq outputs, consisting of gathering FastQC and tag count statistics at the flowcell level, as well as individual FastQC on each sample.

The FastQ files for each sample were aligned to both human reference genome hg19 using STAR (*49*). HTSeq (*50*) was used to obtain transcript counts from the SAM outputs of the STAR alignment using Ensembl gene annotations. The count data were normalized for read depth and analyzed using the DESeq2 package in R, clustering was performed using the pheatmap package, and plots were produced in R and GraphPad Prism. Healthy adult human liver control RNA was obtained commercially (Thermo Fisher and Clonetech).

Statistical analysis

All data are expressed as means ± SEM. Statistical significance ($P < 0.05$) was determined using Student's *t* test (two-sided) or one-way ANOVA, followed by Tukey's post hoc test.

SUPPLEMENTARY MATERIALS

www.sciencetranslationalmedicine.org/cgi/content/full/9/399/eaah5505/DC1

Fig. S1. Bioprinting of scalable liver seed grafts.
Fig. S2. Hepatic aggregates formed from hepatocytes and fibroblasts.
Fig. S3. Liver seed grafts synthesize DNA after partial hepatectomy.
Fig. S4. Global transcriptome of liver seed grafts.
Fig. S5. Liver seed grafts contain cells that express biliary epithelial cell markers.
Fig. S6. Human hepatocyte samples contain rare cytokeratin-19–positive cells.
Fig. S7. Liver seed grafts contain blood vessels lined with human and mouse endothelial cells.
Fig. S8. Liver seed grafts contain rare endothelial cells that express markers associated with the cell cycle.

REFERENCES AND NOTES

1. J. D. Baranski, R. R. Chaturvedi, K. R. Stevens, J. Eyckmans, B. Carvalho, R. D. Solorzano, M. T. Yang, J. S. Miller, S. N. Bhatia, C. S. Chen, Geometric control of vascular networks to enhance engineered tissue integration and function. *Proc. Natl. Acad. Sci. U.S.A.* **110**, 7586–7591 (2013).
2. K. R. Stevens, M. D. Ungrin, R. E. Schwartz, S. Ng, B. Carvalho, K. S. Christine, R. R. Chaturvedi, C. Y. Li, P. W. Zandstra, C. S. Chen, S. N. Bhatia, InVERT molding for scalable control of tissue microarchitecture. *Nat. Commun.* **4**, 1847 (2013).
3. R. P. Visconti, V. Kasyanov, C. Gentile, J. Zhang, R. R. Markwald, V. Mironov, Towards organ printing: Engineering an intra-organ branched vascular tree. *Expert Opin. Biol. Ther.* **10**, 409–420 (2010).
4. J. S. Miller, K. R. Stevens, M. T. Yang, B. M. Baker, D.-H. T. Nguyen, D. M. Cohen, E. Toro, A. A. Chen, P. A. Galie, X. Yu, R. Chaturvedi, S. N. Bhatia, C. S. Chen, Rapid casting of patterned vascular networks for perfusable engineered three-dimensional tissues. *Nat. Mater.* **11**, 768–774 (2012).
5. B. Derby, Printing and prototyping of tissues and scaffolds. *Science* **338**, 921–926 (2012).
6. B.-S. Ding, D. J. Nolan, J. M. Butler, D. James, A. O. Babazadeh, Z. Rosenwaks, V. Mittal, H. Kobayashi, K. Shido, D. Lyden, T. N. Sato, S. Y. Rabbany, S. Rafii, Inductive angiocrine signals from sinusoidal endothelium are required for liver regeneration. *Nature* **468**, 310–315 (2010).
7. F. Lemaigre, K. S. Zaret, Liver development update: New embryo models, cell lineage control, and morphogenesis. *Curr. Opin. Genet. Dev.* **14**, 582–590 (2004).
8. G. K. Michalopoulos, Liver regeneration. *J. Cell. Physiol.* **213**, 286–300 (2007).
9. G. K. Michalopoulos, Principles of liver regeneration and growth homeostasis. *Compr. Physiol.* **3**, 485–513 (2013).
10. Y. Xu, Y. Shi, S. Ding, A chemical approach to stem-cell biology and regenerative medicine. *Nature* **453**, 338–344 (2008).
11. L. Jin, H. Zeng, S. Chien, K. G. Otto, R. E. Richard, D. W. Emery, C. A. Blau, In vivo selection using a cell-growth switch. *Nat. Genet.* **26**, 64–66 (2000).
12. K. R. Stevens, M. W. Rolle, E. Minami, S. Ueno, M. B. Nourse, J. I. Virag, H. Reinecke, C. E. Murry, Chemical dimerization of fibroblast growth factor receptor-1 induces myoblast proliferation, increases intracardiac graft size, and reduces ventricular dilation in infarcted hearts. *Hum. Gene Ther.* **18**, 401–412 (2007).
13. H. Azuma, N. Paulk, A. Ranade, C. Dorrell, M. Al-Dhalimy, E. Ellis, S. Strom, M. A. Kay, M. Finegold, M. Grompe, Robust expansion of human hepatocytes in Fah$^{-/-}$/Rag2$^{-/-}$/Il2rg$^{-/-}$ mice. *Nat. Biotechnol.* **25**, 903–910 (2007).
14. S. Zhu, M. Rezvani, J. Harbell, A. N. Mattis, A. R. Wolfe, L. Z. Benet, H. Willenbring, S. Ding, Mouse liver repopulation with hepatocytes generated from human fibroblasts. *Nature* **508**, 93–97 (2014).
15. N. M. Blackett, S. Hellman, Increased proliferation of transplanted mouse bone marrow cells by pre-irradiation of the recipient. *Nature* **210**, 1284–1285 (1966).
16. E. P. Sandgren, R. D. Palmiter, J. L. Heckel, C. C. Daugherty, R. L. Brinster, J. L. Degen, Complete hepatic regeneration after somatic deletion of an albumin-plasminogen activator transgene. *Cell* **66**, 245–256 (1991).
17. C. Tateno, Y. Yoshizane, N. Saito, M. Kataoka, R. Utoh, C. Yamasaki, A. Tachibana, Y. Soeno, K. Asahina, H. Hino, T. Asahara, T. Yokoi, T. Furukawa, K. Yoshizato, Near completely humanized liver in mice shows human-type metabolic responses to drugs. *Am. J. Pathol.* **165**, 901–912 (2004).
18. T. Takebe, K. Sekine, M. Enomura, H. Koike, M. Kimura, T. Ogaeri, R.-R. Zhang, Y. Ueno, Y.-W. Zheng, N. Koike, S. Aoyama, Y. Adachi, H. Taniguchi, Vascularized and functional human liver from an iPSC-derived organ bud transplant. *Nature* **499**, 481–484 (2013).
19. J. Ding, G. R. Yannam, N. Roy-Chowdhury, T. Hidvegi, H. Basma, S. I. Rennard, R. J. Wong, Y. Avsar, C. Guha, D. H. Perlmutter, I. J. Fox, J. Roy-Chowdhury, Spontaneous hepatic repopulation in transgenic mice expressing mutant human α1-antitrypsin by wild-type donor hepatocytes. *J. Clin. Invest.* **121**, 1930–1934 (2011).
20. S. R. Khetani, S. N. Bhatia, Microscale culture of human liver cells for drug development. *Nat. Biotechnol.* **26**, 120–126 (2008).

21. A. A. Chen, D. K. Thomas, L. L. Ong, R. E. Schwartz, T. R. Golub, S. N. Bhatia, Humanized mice with ectopic artificial liver tissues. *Proc. Natl. Acad. Sci. U.S.A.* **108**, 11842–11847 (2011).
22. C. S. Chen, M. Mrksich, S. Huang, G. M. Whitesides, D. E. Ingber, Geometric control of cell life and death. *Science* **276**, 1425–1428 (1997).
23. E. E. Hui, S. N. Bhatia, Micromechanical control of cell-cell interactions. *Proc. Natl. Acad. Sci. U.S.A.* **104**, 5722–5726 (2007).
24. E. M. Wilson, J. Bial, B. Tarlow, G. Bial, B. Jensen, D. L. Greiner, M. A. Brehm, M. Grompe, Extensive double humanization of both liver and hematopoiesis in FRGN mice. *Stem Cell Res.* **13**, 404–412 (2014).
25. Y. P. de Jong, M. Dorner, M. C. Mommersteeg, J. W. Xiao, A. B. Balazs, J. B. Robbins, B. Y. Winer, S. Gerges, K. Vega, R. N. Labitt, B. M. Donovan, E. Giang, A. Krishnan, L. Chiriboga, M. R. Charlton, D. R. Burton, D. Baltimore, M. Law, C. M. Rice, A. Ploss, Broadly neutralizing antibodies abrogate established hepatitis C virus infection. *Sci. Transl. Med.* **6**, 254ra129 (2014).
26. B. C. Yan, C. Gong, J. Song, T. Krausz, M. Tretiakova, E. Hyjek, H. Al-Ahmadie, V. Alves, S.-Y. Xiao, R. A. Anders, J. A. Hart, Arginase-1: A new immunohistochemical marker of hepatocytes and hepatocellular neoplasms. *Am. J. Surg. Pathol.* **34**, 1147–1154 (2010).
27. P. van Eyken, R. Sciot, B. van Damme, C. de Wolf-Peeters, V. J. Desmet, Keratin immunohistochemistry in normal human liver. Cytokeratin pattern of hepatocytes, bile ducts and acinar gradient. *Virchows Arch. A Pathol. Anat. Histopathol.* **412**, 63–72 (1987).
28. J. Hu, K. Srivastava, M. Wieland, A. Runge, C. Mogler, E. Besemfelder, D. Terhardt, M. J. Vogel, L. Cao, C. Korn, S. Bartels, M. Thomas, H. G. Augustin, Endothelial cell-derived angiopoietin-2 controls liver regeneration as a spatiotemporal rheostat. *Science* **343**, 416–419 (2014).
29. B.-S. Ding, Z. Cao, R. Lis, D. J. Nolan, P. Guo, M. Simons, M. E. Penfold, K. Shido, S. Y. Rabbany, S. Rafii, Divergent angiocrine signals from vascular niche balance liver regeneration and fibrosis. *Nature* **505**, 97–102 (2014).
30. K. Matsumoto, H. Yoshitomi, J. Rossant, K. S. Zaret, Liver organogenesis promoted by endothelial cells prior to vascular function. *Science* **294**, 559–563 (2001).
31. F. L. Moolten, N. L. R. Bucher, Regeneration of rat liver: Transfer of humoral agent by cross circulation. *Science* **158**, 272–274 (1967).
32. T. Hoppo, J. Komori, R. Manohar, D. B. Stolz, E. Lagasse, Rescue of lethal hepatic failure by hepatized lymph nodes in mice. *Gastroenterology* **140**, 656–666.e2 (2011).
33. J. Komori, L. Boone, A. DeWard, T. Hoppo, E. Lagasse, The mouse lymph node as an ectopic transplantation site for multiple tissues. *Nat. Biotechnol.* **30**, 976–983 (2012).
34. A. Soto-Gutiérrez, N. Kobayashi, J. D. Rivas-Carrillo, N. Navarro-Álvarez, D. Zhao, T. Okitsu, H. Noguchi, H. Basma, Y. Tabata, Y. Chen, K. Tanaka, M. Narushima, A. Miki, T. Ueda, H.-S. Jun, J.-W. Yoon, J. Lebkowski, N. Tanaka, I. J. Fox, Reversal of mouse hepatic failure using an implanted liver-assist device containing ES cell-derived hepatocytes. *Nat. Biotechnol.* **24**, 1412–1419 (2006).
35. R. Zhao, S. A. Duncan, Embryonic development of the liver. *Hepatology* **41**, 956–967 (2005).
36. C. Schmidt, F. Bladt, S. Goedecke, V. Brinkmann, W. Zschiesche, M. Sharpe, E. Gherardi, C. Birchmeier, Scatter factor/hepatocyte growth factor is essential for liver development. *Nature* **373**, 699–702 (1995).
37. G. A. Kwong, G. von Maltzahn, G. Murugappan, O. Abudayyeh, S. Mo, I. A. Papayannopoulos, D. Y. Sverdlov, S. B. Liu, A. D. Warren, Y. Popov, D. Schuppan, S. N. Bhatia, Mass-encoded synthetic biomarkers for multiplexed urinary monitoring of disease. *Nat. Biotechnol.* **31**, 63–70 (2013).
38. S. Nissim, R. I. Sherwood, J. Wucherpfennig, D. Saunders, J. M. Harris, V. Esain, K. J. Carroll, G. M. Frechette, A. J. Kim, K. L. Hwang, C. C. Cutting, S. Elledge, T. E. North, W. Goessling, Prostaglandin E_2 regulates liver versus pancreas cell-fate decisions and endodermal outgrowth. *Dev. Cell* **28**, 423–437 (2014).
39. J. Shan, R. E. Schwartz, N. T. Ross, D. J. Logan, D. Thomas, S. A. Duncan, T. E. North, W. Goessling, A. E. Carpenter, S. N. Bhatia, Identification of small molecules for human hepatocyte expansion and iPS differentiation. *Nat. Chem. Biol.* **9**, 514–520 (2013).
40. B. D. Tarlow, C. Pelz, W. E. Naugler, L. Wakefield, E. M. Wilson, M. J. Finegold, M. Grompe, Bipotential adult liver progenitors are derived from chronically injured mature hepatocytes. *Cell Stem Cell* **15**, 605–618 (2014).
41. G. K. Michalopoulos, L. Barua, W. C. Bowen, Transdifferentiation of rat hepatocytes into biliary cells after bile duct ligation and toxic biliary injury. *Hepatology* **41**, 535–544 (2005).
42. S. N. Bhatia, G. H. Underhill, K. S. Zaret, I. J. Fox, Cell and tissue engineering for liver disease. *Sci. Transl. Med.* **6**, 245sr2 (2014).
43. R. L. Jirtle, C. Biles, G. Michalopoulos, Morphologic and histochemical analysis of hepatocytes transplanted into syngeneic hosts. *Am. J. Pathol.* **101**, 115–126 (1980).
44. K. R. Stevens, J. S. Miller, B. L. Blakely, C. S. Chen, S. N. Bhatia, Degradable hydrogels derived from PEG-diacrylamide for hepatic tissue engineering. *J. Biomed. Mater. Res. A* **103**, 3331–3338 (2015).
45. T. Takebe, K. Sekine, M. Enomura, H. Koike, M. Kimura, T. Ogaeri, R. R. Zhang, Y. Ueno, Y. W. Zheng, N. Koike, S. Aoyama, Y. Adachi, H. Taniguchi, Vascularized and functional human liver from an iPSC-derived organ bud transplant. *Nature* **499**, 481–484 (2013).
46. T. C. McDevitt, M. A. Laflamme, C. E. Murry, Proliferation of cardiomyocytes derived from human embryonic stem cells is mediated via the IGF/PI 3-kinase/Akt signaling pathway. *J. Mol. Cell. Cardiol.* **39**, 865–873 (2005).
47. C. Mitchell, H. Willenbring, A reproducible and well-tolerated method for 2/3 partial hepatectomy in mice. *Nat. Protoc.* **3**, 1167–1170 (2008).
48. E. Murray, J. H. Cho, D. Goodwin, T. Ku, J. Swaney, S.-Y. Kim, H. Choi, Y.-G. Park, J. Y. Park, A. Hubbert, M. McCue, S. Vassallo, N. Bakh, M. P. Frosch, V. J. Wedeen, H. S. Seung, K. Chung, Simple, scalable proteomic imaging for high-dimensional profiling of intact systems. *Cell* **163**, 1500–1514 (2015).
49. A. Dobin, C. A. Davis, F. Schlesinger, J. Drenkow, C. Zaleski, S. Jha, P. Batut, M. Chaisson, T. R. Gingeras, STAR: Ultrafast universal RNA-seq aligner. *Bioinformatics* **29**, 15–21 (2013).
50. S. Anders, P. T. Pyl, W. Huber, HTSeq—A Python framework to work with high-throughput sequencing data. *Bioinformatics* **31**, 166–169 (2015).

Acknowledgments: We thank A. Sappington for help with bioinformatics analysis, L. Wilson of Yecuris for advice regarding animal care, the Koch Institute BioMicroCenter for help with library sequencing, and the Swanson Biotechnology Center Microscopy Core for help with imaging. **Funding:** This study was supported by grants from the NIH (R01EB008396, R01DK85713, EB00262, U24DK059635, and P30-CA14051), the Skolkovo Institute of Science and Technology (022423-003), and the National Institute of Environmental Health Sciences (P30-ES002109). M.A.S. was supported by the National Research Service Award (F32AI091207), and K.A.K. was supported by the National Institute of General Medical Sciences Training Grant (T32GM007753). S.N.B. is a Howard Hughes Medical Institute investigator. **Author contributions:** K.R.S., M.A.S., V.R., C.L.F., R.R.C., K.A.K., J.W.X., C.F., T.M., A.X.C., M.G.M., M.T.Y., Y.P.d.J., and H.E.F. designed and performed all experiments. M.A.S., M.T.Y., Y.P.d.J., R.R.C., J.W.X., C.F., T.M., and C.L.F. designed and performed the transplant experiments. V.R. designed and analyzed the transcriptome experiments. K.A.K. designed and performed the partial hepatectomy experiments. M.G.M. and K.C. designed and performed the lectin analysis experiments. K.R.S., H.E.F., C.S.C., C.M.R., and S.N.B. wrote the paper. K.C., Y.P.d.J., C.S.C., C.M.R., and S.N.B. provided funding, contributed to experiment planning, and provided overall oversight of the study. **Competing interests:** S.N.B. is a co-founder of Hepregen. C.S.C. is co-founder of Innolign Biomedical. K.R.S., C.S.C., and S.N.B. are co-inventors on a patent entitled "SEEDs (in situ expansion of engineered devices) for templated regeneration" (#PCT/US2016/055972).

Submitted 17 July 2015
Resubmitted 12 July 2016
Accepted 6 March 2017
Published 19 July 2017
10.1126/scitranslmed.aah5505

Citation: K. R. Stevens, M. A. Scull, V. Ramanan, C. L. Fortin, R. R. Chaturvedi, K. A. Knouse, J. W. Xiao, C. Fung, T. Mirabella, A. X. Chen, M. G. McCue, M. T. Yang, H. E. Fleming, K. Chung, Y. P. de Jong, C. S. Chen, C. M. Rice, S. N. Bhatia, In situ expansion of engineered human liver tissue in a mouse model of chronic liver disease. *Sci. Transl. Med.* **9**, eaah5505 (2017).

Science Translational Medicine

In situ expansion of engineered human liver tissue in a mouse model of chronic liver disease

Kelly R. Stevens, Margaret A. Scull, Vyas Ramanan, Chelsea L. Fortin, Ritika R. Chaturvedi, Kristin A. Knouse, Jing W. Xiao, Canny Fung, Teodelinda Mirabella, Amanda X. Chen, Margaret G. McCue, Michael T. Yang, Heather E. Fleming, Kwanghun Chung, Ype P. de Jong, Christopher S. Chen, Charles M. Rice and Sangeeta N. Bhatia

Sci Transl Med **9**, eaah5505.
DOI: 10.1126/scitranslmed.aah5505

Tissue seeds blossom after transplant

There is an enormous clinical need for liver transplant tissue. Bioengineered livers might ultimately be used as a bridge to or alternative for whole organ transplantation. In new work, Stevens *et al*. fabricated human artificial liver "seeds" in biomaterials that were able to grow and expand after implantation into mice in response to liver injury. After growth, the human artificial liver seeds were able to carry out normal liver functions such as production of human proteins like transferrin and albumin. This study suggests that implanted engineered tissue seeds should be able to expand in response to the body's own repair signals.